ISSN 1349-1148
JAXA-RR-03-020E

JAXA Research and Development Report

Scramjet Performance Achieved in Engine Tests from M4 to M8 Flight Conditions

March 2004

Japan Aerospace Exploration Agency

JAXA-RR-03-020E

JAXA Research and Development Report
宇宙航空研究開発機構研究開発報告

Scramjet Performance Achieved in Engine Tests from M4 to M8 Flight Conditions

M4からM8におけるスクラムジェットエンジン試験における性能達成度

Tohru MITANI [*1], Sadatake TOMIOKA [*1], Takeshi KANDA [*1], Nobuo CHINZEI [*1], Toshinori KOUCHI [*2]
三谷 徹、富岡 定毅、苅田 丈士、鎮西 信夫、河内 俊憲

*1: Space Propulsion Research Center
Institute of Space Technology and Aeronautics
総合技術研究本部 宇宙推進技術共同センター

*2: Tohoku University, Department of Aeronautics and Space Engineering
東北大学 大学院 航空宇宙工学専攻

March 2004
2004年3月

Japan Aerospace Exploration Agency
宇宙航空研究開発機構

Scramjet Performance Achieved in Engine Tests from M4 to M8 Flight Conditions*

Tohru MITANI,[*1] Sadatake TOMIOKA,[*1] Takeshi KANDA,[*1]
Nobuo CHINZEI,[*1] and Toshinori KOUCHI[*2]

Abstract

Thrust performances of scramjet engines were compared with theoretical values to quantify the progress in engine performances (defined as "achievement factors", or "factors") from Mach (termed as "M") 4 to M8 flight conditions. An engine with a ramp produced a net thrust of 215 N under the M8 tests and a comparison of a theoretical thrust yielded a thrust achievement factor of 51%. By excluding boundary layer, an engine with a thick strut delivered a net thrust of 560 N and showed a thrust factor of 92% and a net thrust factor of 45%. The thrusts were limited by flow separation caused by engine combustion (termed as "engine unstart"). The starting characteristics was improved by boundary layer controls in M6 and M4 conditions. An engine with a thin strut doubled the thrust from 1620 N to 2460 N by the boundary layer bleeding in the M6 tests. The improved thrust factor was 60% at the stoichiometric H_2 condition. Under M4 tests, the net thrust was tripled by the bleed and a two-staged injection of H_2. As results, the thrust factor was raised from 53% to 70%, the net thrust factor was increased from 32% to 55%. Studies required for improving the net performance were addressed.

Nomenclature

A_1	Inlet entrance area (width 0.2 m×height 0.25 m)
cf	wall friction coefficient
C_{int}	Internal drag coefficient of engines (= Cdp + Cdf)
D_{air}	air drag of engines (N)
D_{int}	Internal drag of engines (= $C_{int} \cdot q_1 \cdot A_1$) (N)
Df	Internal friction drag on engines (N)
Df_0	Minimum friction drag on the internal surface of a rectangular duct (N)
Dp	Internal pressure drag of engines (N)
d_1	Displacement thickness of boundary layer swallowed by engines (mm)
Isp	Fuel specific impulse (km/s)
M	Mach number
q_1	Freestream dynamic pressure at the inlet (kPa)
η_p	Total pressure recovery factor
η_c	Air capture ratio in inlets
ΔF	Thrust increment by combustion (N)
ΔF_{net}	Net thrust by combustion (= $\Delta F - D_{int}$) (N)
η_{drag}	Drag achievement factor (= Df_0/D_{int})
$\eta_{\Delta F}$	Thrust achievement factor (= $\Delta F_{exp} / \Delta F_0$)
η_{net}	Net thrust achievement factor (= $(\Delta F_{exp} - D_{int})/(\Delta F_0 - Df_0)$)
ε	Geometrical contraction ratio of inlets
Φ	H_2 equivalence ratio
subscripts	
exp	experimental values
0	baseline values

* received 13 January, 2004（平成16年1月13日）

*1 Space Propulsion Research Center, Institute of Space Technology and Aeronautics
（総合技術研究本部 宇宙推進技術共同センター）

*2 Tohoku University, Department of Aeronautics and Space Engineering
（東北大学大学院 航空宇宙工学専攻）

Introduction

Development of hydrogen (H_2)-fueled scramjet engines is being undertaken under flight conditions of Mach 4, 6 and 8 using the RamJet engine Test Facility (RJTF) at National Aerospace Laboratory, Japan. In the engine tests, our engines delivered net thrusts which overcame the engine drag under Mach 4 to 8 flight conditions. However, the thrust was limited by the occurrence of inlet unstart (termed "engine unstart" or simply "unstart") due to combustion. It is caused by the boundary layer separation in inlets of engines. Therefore, boundary layer bleeding and two-staged injection of H_2 were examined to extend the engine operational range to $\Phi = 1$. Details of our previous work, the facility employed and the engine testing are described in Ref. 1, and recent progress can be found in Refs. 2 to 6.

This paper has four objectives;

1) Examinations of accuracy of our thrust measurements
2) Reviews of our M4 to M8 engine performance
3) Quantification of the thrust, net thrust performances achieved in our engine tests,
4) Drag reduction for improving the net performance.

Two thrust measurements, namely one by a Force Measurement System (FMS) and the other by wall pressure integration are explained to facilitate the accuracy of our engine testing. Engine data about the thrusts and the specific impulse are reviewed in the M4, M6 and M8 conditions. To improve engine performance, it is necessary to compare the engine data with values obtained theoretically. Therefore, fast fuel mixing and combustion distributed downstream of the engine throat are assumed to calculate the theoretical performance.[7] Comparison of the engine data with the theoretical values enables quantification of the engine performances achieved under Mach 4, 6 and 8 flight conditions. These performances with regard to combustion, net thrust and engine drag are discussed.

Engine Geometry and Analysis

H_2-fueled Scramjet Engines and Test Conditions

Two side-compression-type scramjet engines were constructed in our testing. These engines can be quickly and easily reconfigured so that various struts and ramps in the engines can be tested. The engines are all rectangular and consist of a cowl, a topwall and two sidewalls (Fig. 1). The entrance and the exit of the engine are 200 mm wide, 250 mm high (denoted by H) and 2.1 m long. The inlet is a sidewall compression type with a 6-degree half angle. The engines have a swept-back angle of 45 degrees to deflect the airstream for suitable spillage required in starting. The baseline engine has the swept back angle throughout the engine (named E1 engine). The geometrical contraction ratio is 2.86 without struts. Inlets with struts and ramps were tested to examine the inlet and combustion performances.[1]

Since severe distortions of air and H_2 flows were detected by gas sampling in the E1 engines, a new engine (named E2 engine), which is illustrated in the lower part in Fig. 1, was constructed.2 The swept-back angle is eliminated downstream of the isolator in order to minimize the distortion of the airflow. In some M8 tests, a 1.23-m long, 250-mm high, 46-mm thick strut was installed in the combustor and diverging section (the geometrical contraction ratio is 8.33). Instead of the strut, a compression ramp with a contraction ratio of 7.94 was also tested. This engine is cooled by sparsely-distributed water channels so that precise measurements of distributions of wall pressure and heating rate are possible. The E1 and E2 engines

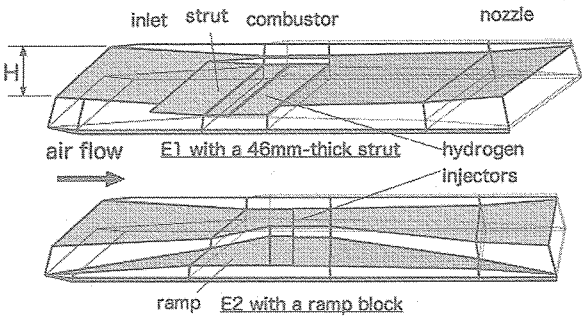

Fig. 1 Engine with a strut (E1) and engine with a ramp (E2).

were tested in the Mach 8 tests, while only the E1 engine was employed in the Mach 4 and 6 tests.

The test conditions and summaries of engine performances are presented in Table 1, where the inlet Mach number (M_1), the displacement thickness of the ingested boundary layer (d_1 in mm), the geometric contraction ratio (ε) and the air capture ratio (η_c) are shown. The lower Mach numbers represent the engine inlet conditions behind the bow shock of the vehicles. The engines are mounted in a test cell so as to ingest the facility nozzle boundary layer which simulates the effects of vehicle forebody boundary layer ingestion in flight.

The mass rate (Ma in kg/s) of air passing through the inlet is dependent on the boundary layer swallowed by the engines. For example, the air mass rate in the engines with the 5/5H strut is 1.29 kg/s with boundary layer ingestion in the M8 condition, and the mass flow rate increases to 1.48 kg/s by excluding the boundary layer. Boundary layer exclusion was achieved by moving the engine to the core region of the facility nozzle. Since engines easily fell into the unstart due to combustion, the effects of boundary layer bleeding were investigated in the M6 and M4 tests. In the M4 tests, the mass rate of air flowing into the inlet is the same (6.7 kg/s). However, the air flow rate in the combustor decreases by 0.2 kg/s in Table 1. The bleed-air rate in the M6 test is small so that the air flow rate to combustor is unchanged (5.0 kg/s)

The stoichiometric H_2 rate in Table 1 is determined by the air flow rates and found to be from 42 g/s (M8-strut engine) to 195 g/s (M4-strutless engine). The H_2 was injected normally from the sidewalls through 24 fuel orifices in the combustor. In some Mach 4 tests, two-staged injection of H_2 was examined to improve the thrust performance where the additional H_2 was injected at 558 mm downstream of the combustor step.

Internal drag (D_{int}) of the engines and minimum friction drag of rectangular ducts (Df_0) are listed in Table 1. Thrust produced by combustion in engine tests (ΔF_{exp}), i.e., the axial force of the engine with combustion minus the axial force on engine with no fuel injection (called *air-drag*, D_{air}), is a key performance. The counterparts estimated by one-dimensional analysis (ΔF_{1D}) are shown for the tested H_2 equivalence ratio (Φ). The net thrust is defined by ΔF - D_{int} and the fuel specific impulse (Isp) is calculated from the net thrust and the fuel supply rate. Definitions of the performance achievement factors of thrust ($\eta_{\Delta F}$), net thrust (η_{net}) and drag (η_{drag}) are discussed later.

Thrust Measured by a Force Balance

In our facility, forces acting on engines were measured by a balance (Force Measuring System, FMS) consisting of a floating frame supported by a thrust load-cell (the full-range: 8.9 kN) and three load-cells (22 kN) for lift and pitching moment. The FMS contains a calibration system driven by oil pressure and can revise the calibration matrix under conditions of installation of fuel and cooling water supply lines and measurement cables.

This FMS measurement is a steady-state measurement in which test conditions are maintained from two seconds to ten seconds for each H_2 rate; the signal/noise ratio is high. The baseline of FMS before and that after each wind tunnel blowdown are compared to check baseline shifts sometimes caused by thermal stress in engines in the hot airflow. At first in tests, engine drag caused by airflow (D_{air}) is measured without the fuel supply. The

Table 1 Test conditions, thrust measured and achievement factors of engine performance.

	test case	M1	d_1, mm	ε	ηc	Ma, kg/s	M)H_2, g/s	D_{int}, N	Df_0, N	Φ	ΔF1D	ΔFexp	Fnet, N	Isp)f, km/s	$\eta_{\Delta F}$	η_{net}	η_{drag}
I	M8 with 5/5H-strut	6.7	32.8	8.33	0.74	1.29	41.6	660	90	0.42	429	316	-344	-	0.74	-	0.14
II	without BL	6.7	0.0	8.33	0.74	1.48	47.9	660	90	2.10	1325	1220	560	5.6	0.92	0.45	0.14
III	M8 with ramp	6.7	32.8	7.94	0.80	1.39	44.9	295	90	1.20	1009	510	215	4.0	0.51	0.23	0.31
IV	without BL	6.7	0.0	7.94	0.80	1.60	51.7	295	90	1.30	1200	760	465	6.9	0.63	0.42	0.31
V	M6 with 5/5H-strut	5.3	19.7	5.00	0.80	5.00	145.0	784	270	0.48	2530	1620	836	12.0	0.64	0.37	0.34
VI	0.6%-bleed & staged H_2	5.3	19.7	5.00	0.80	5.00	145.0	784	270	1.00	4070	2460	1676	11.6	0.60	0.44	0.34
VII	M4 without strut	3.4	11.7	2.86	0.72	6.70	195.0	570	280	0.30	2250	1200	630	10.8	0.53	0.32	0.49
VIII	3%-bleed & staged H_2	3.4	-	2.86	0.72	6.50	195.0	700	280	0.95	3660	2560	1860	10.0	0.70	0.55	0.40

air-drag are monitored before and after individual combustion sequences to examine the reproducibility of measurements.

Figure 2 illustrates a force measurement in our M6 test[6] in which variations of the thrust (left-hand side) and H_2 equivalence ratio (right-hand side) are plotted. In Fig. 2, the nozzle flow was established at 36 sec, at which the air-drag was measured to be 1340 N. Then the drag decreases and thrust was produced stepwise due to engine combustion when the H_2 was supplied from 40.5 sec. The H_2 rate was varied sequencially between Φ = 0.21 and 1.22 (corresponding to H_2 flow rate of 177 g/s) in this experiment. The maximum thrust reading was found to be Fx = 1050 N at 49 sec at Φ = 1. Just after attaining it, the engine fell to the unstart and the reading showed a drag of -1150 N with the same H_2 rate. It implies that the H_2 flow rate is the limit for engine operation. The unstart continued at Φ = 1.22 till 52.5 sec. A self-restarting of engine, caused by the tailing-off of fuel, is observed at 53 sec. The engine test was completed at 53 sec and the D_{air} was measured at 55 sec again to monitor drifts in the FMS readings.

Following performance properties are defined by using Fig. 2. Combustion performance is indicated by a thrust increment measured from the D_{air} and the increment is termed *thrust by combustion* or simply thrust (ΔF) here. Since D_{air} = 1410 N, the maximum thrust was found to be 2460 N at Φ = 1 at 49 sec. The D_{air} consists of two drags, namely *internal drag* (D_{int}) worked on the internal walls in

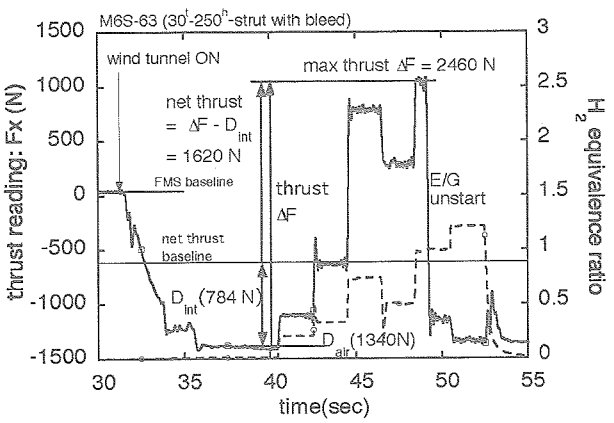

Fig. 2 Variation s of thrust, net thrust and H_2 supply rate.

engines and *external drag* on the external surfaces. The external drag depends on the external geometry and decreases when engine modules are clustered. On the other hand, the D_{int} is related to irreversible processes, such as spill drag, total pressure loss in inlets and friction loss in engines, and it is the most important, intrinsic property for evaluating engine performance. Therefore, net thrust is defined as $\Delta F - D_{int}$. Because D_{int} of the engine in Fig. 2 was 784 N, the maximum thrust was measured to be 1620 N .

Thrust Measured by Wall Pressure Integration

The air-drag measured by the FMS includes the external drag in addition to the D_{int}. Mitani et al. have proposed a method to evaluate the pressure drag (Dp) and the friction drag (Df) on internal walls of engines based on wall pressure measurements[8] and examined its accuracy in various engine geometries and flight conditions.[9]

Figures 3 illustrate wall pressure distributions with and without combustion measured in an engine with a 30-mm-thick strut in the M6 condition. The wall pressure is nondimensionalized by the dynamic pressure in the freestream (107 kPa at the nozzle total pressure of 4.8 MPa). The dotted points are measurement stations on the sidewall of the engine. The total number of the points measured is about 150 on the sidewall, the topwall, the cowl and the strut.

Figure 3a shows the isobaric contour lines before injection of H_2. A shockwave generated at the leading wedge of the sidewall impinges at the fifth row of measurement points to form a high pressure region of 0.2 at the exit of the inlet, where the static pressure is 0.05 at the entrance of inlet. The shock wave increases the wall pressure in the isolator section to 0.8 in Fig. 3a. Spilled flow in the swept-back inlet deflected back horizontally produces a strong cowl shock which propagates toward the topwall. The maximum pressure of 1.35 is observed behind the cowl shock in Fig. 3a. The airflow is accelerated in the diverging combustor section and the wall pressure decreases to 0.1 (11 kPa) at the nozzle exit.

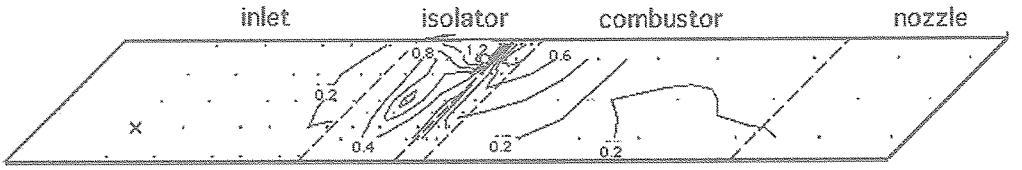

(a) without combustion (min = 0.048: X, max = 1.35: O)

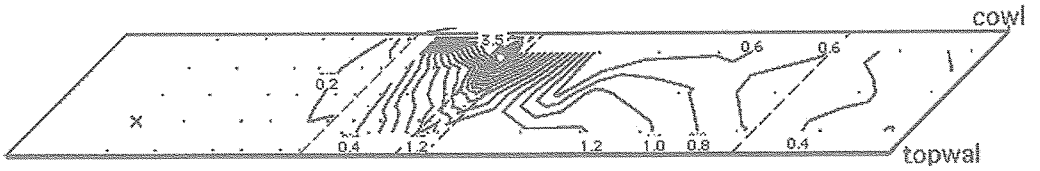

(b) with combustion of F=1.0 (min = 0.053: X, max = 4.12: O)

Fig. 3 Wall pressure distributions (E1 - struted engine with boundary-layer bleed in the M6).

Figure 3b is the pressure distribution obtained in an engine delivering thrust of 2460 N with a H_2 supply rate of Φ = 1 (see at 48 sec in Fig. 2). There is no change in the inlet which is occupied by a supersonic flow. A high pressure region is formed just behind the injector section and the maximum pressure increases from 1.35 (140 kPa) in the air condition to 4.12 (430 kPa) near the combustor. Comparison between Fig. 3a and Fig. 3b indicates that the high pressure region is formed in the isolator due to combustion. However, the raised pressure is confined near the cowl side and it does not affect the pressure field near the topwall at the rear of the isolator. This is attributed to the small boundary layer bleed of 30 g/s. It was found in cases without bleed that the high pressure region easily penetrated the isolator section to the inlet resulting the engine unstart.

The wall pressure at the entrance of the diverging combustor section is raised from 0.2 (215 kPa) to 4.12 (440 kPa) by combustion and the high pressure produces the thrust. Integrations of the wall pressure shown in Figs. 3 yield another ΔF, which can be compared with the counterpart obtained by the FMS. The FMS measurements are contaminated by the external drag. However, the thrust from wall pressure are determined only by the internal flow in engines.

In order to examine consistency between the two ΔF, their correlation is plotted in Fig. 4. The data symbols denote different test conditions, for instance, the "1bld" imply "H_2 injected from No.1 port with the boundary layer bleed". While the ΔF measured by FMS contains the friction drag worked on the engine, the ΔF obtained from the wall pressure integration does not. Therefore, the two ΔF with and without combustion differ by changes in friction force due to the combustion. An increase of the friction drag by combustion decreases ΔF measured by FMS. Therefore, effects of combustion on the ΔF were investigated.

Combustion reduces the Reynolds number and Mach number inside engines and increases wall friction coefficients, cf. On the other hand, combustion decreases dynamic pressure in engine internal flows. Assuming a complete combustion at Φ = 1,

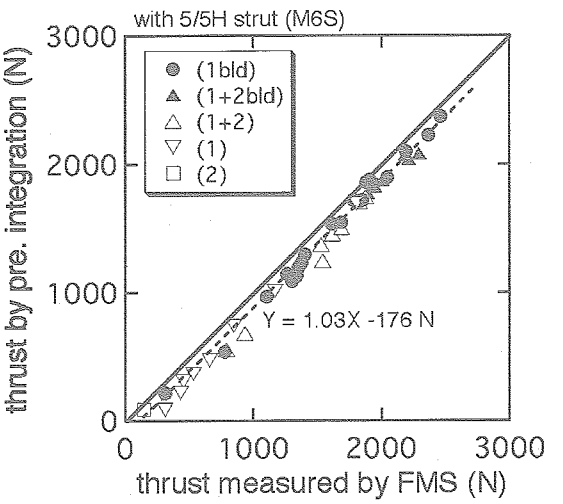

Fig. 4 Correlation between ΔF by FMS and ΔF by wall pressure integration.

increments in the friction drag due to combustion are 30 N in the engine without struts (M4), 116 N in the engine with a 30-mm-thick, 5/5H-high strut (M6) and 60 N in the engine with a ramp (M8). Therefore, we expected that the correlation data should be scattered along a line of Y = 0.98X in Fig. 4. However, all the data were correlated by Y = 1.03X - 176. Considering experimental errors (±100 N) including repeatabilities of engine tests, the discrepancy of 5% in the slope is within the errors. Thus, Figure 4 indicates the reliability and accuracies of the two, independent thrust measurements. It also shows that the external flow of engine does not contaminate our FMS measurements.

Quantification of Achieved Performances

One-Dimensional Analysis and Assumptions

The flow field is supersonic in scramjet engines and the flow upstream of the combustors is not affected by combustion. Therefore, thrust delivered in expansion sections downstream of the combustor can be calculated by any reactive flow calculations. In this study, our two in-house codes assuming chemical equilibrium flow were used and effects of quenching of dissociated species in low-pressure flow were investigated by a one-dimensional reactive flow code.[8] The upstream boundary conditions at the engine throat were evaluated from experimental data from the subscaled wind tunnel.[6,7] The increment of thrust from the value under the airflow condition corresponds to the ΔF obtained in engine tests. Experimental values (ΔF_{exp} in N), theoretical values (ΔF_{1D} in N), corresponding H_2 flow rates (m_{H2} in g/s) and fuel specific impulses (Isp in km/s) are summarized in Table 1.

Since the total pressure loss by heating (Rayleigh loss) becomes significant and dependent on combustion in engines, theoretically-available thrusts are not uniquely defined. As a result, the combustion schedule must be specified to calculate the performance. Concentrated combustion at the engine throat yields the maximum thrust if the supersonic condition is satisfied in engine flow. However, this high combustion rate easily causes thermal choking in engines operating at lower Mach numbers. In addition, this thermal choking also restricts the operation in engines in high Mach number flights, because these engines require higher compression ratios for combustion.

In order to evaluate the maximum thrust as baseline data, the ΔF_{1D} was calculated under two assumptions: an infinitely fast mixing of fuel by the combustor entrance and a distributed combustion downstream of the throat in which the combustion proceeded with M = 1 being maintained in the diverging section.[7] This *distributed combustion* minimizes the Rayleigh loss and avoids the thermal choking in supersonic combustion engines. Validity of these assumptions will be discussed in comparison with our experimental data later.

Achievement Factors of Engine Performance

In order to evaluate how good or bad our engine performances are, the achievement factors of combustion and net thrust are quantified. The thrust achievement factor ($\eta_{\Delta F}$) is defined by comparing the experimental thrust with the one-dimensional thrust. This reflects the combustion performance in engines.

$$\eta_{\Delta F} = \Delta F_{exp} / \Delta F_{1D} \qquad (1)$$

Although ΔF represents the combustion performance of the engine, it does not directly indicate the net performance of engines. For instance, a large flameholder in combustors enhances combustion. However, It increases the engine drag, resulting in loss of thrust propelling vehicles. Net thrust is defined by the thrust increment by combustion minus the internal drag. For a net thrust achievement factor (η_{net}), the numerator is evaluated based on the experimental thrust and the measured internal drag. The denominator giving the maximum net thrust is defined by using the one-dimensional thrust and a minimum internal drag (Df_0).

$$\eta_{net} = \left(\Delta F_{exp} - D_{int}\right) / \left(\Delta F_{1D} - Df_0\right) \qquad (2)$$

The minimum drag is evaluated using an ideal engine consisting of four flat plates, the drag of

which is only friction. All the waves are canceled out in the ideal engine such that no pressure drag exists. The details will be discussed in a later section.

Engine Performance Attained in RJTF Tests

Mach 8 Condition

Engines with struts

Figure 5 presents the ΔF_{1D} and ΔF_{exp} measured in the engine with the 46-mm-thick strut.[2] The η_c and the η_p necessary for the calculations were measured in subscaled wind tunnel tests. One-dimensional analysis indicates that thrust increases with the Φ and thermal choking occurs near $\Phi = 1$ if H_2 fuel completely burns at the throat. The distributed combustion yields a thrust of 880 N at $\Phi = 1$ and shows increasing thrust beyond $\Phi = 1$ due to mass addition and molecular weight reduction by H_2. The engine was choked at about $\Phi = 6$ in the distributed combustion mode by the H_2 addition.

Engine data for various engine configurations are plotted in Fig. 5. The solid data denote results obtained from the E2 engine and the open symbols are for the E1 engine. The solid circles for the engine with the large 46-mm thick strut show the highest combustion performance close to the theoretical line at a given Φ. However, the engine falls into inlet unstart after attaining the maximum thrust of 316 N at $\Phi = 0.42$. A maximum thrust of 425 N at $\Phi = 1.4$ is observed in the E1 engine with a 46-mm-thick, 637-mm-long strut (open diamonds).

Engine thrust varies depending on the strut geometries and H_2 injection patterns. When a 1229-mm-long strut is installed (solid triangles), the thrust increases. However, the engine easily falls to the unstart condition at $\Phi = 0.6$. When H_2 is concentratedly injected near the cowl, combustion deteriorates (solid squares). Generally speaking, larger struts enhance combustion and the resulting better combustion performance promotes the inlet unstart. If the performances are evaluated using the best ΔF_{exp} (316 N at $\Phi = 0.42$) of the solid circle and the corresponding ΔF_{1D} (429 N), the $\eta_{\Delta F}$ is 74%.

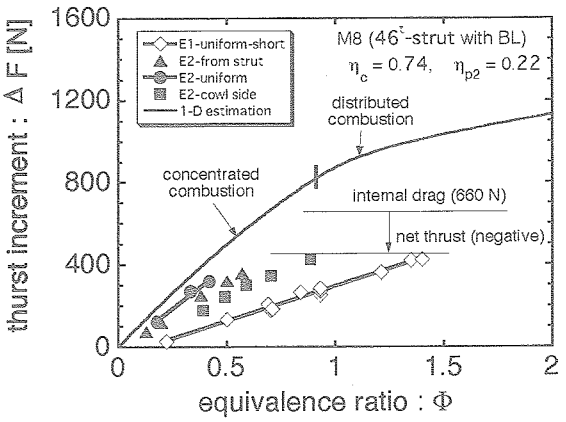

Fig. 5 Measured thrusts and the comparison with analytical value (M8 - 46-mm-thick struted engine).

The D_{int} (660 N) of the E2 engine with the 46-mm-thick strut is also indicated by the horizontal line. If this drag is subtracted from the best ΔF_{exp} of 316 N, the ΔF_{net} for the solid circle becomes a negative value of -344 N. Although the engine with large strut shows the better combustion performance, the large strut increases D_{int} resulting in loss of ΔF_{net}. For engines with struts, it is necessary to reduce the D_{int} and to extend the engine operation range to $\Phi = 1$.

Engine with Ramp

Thrust and drag performances in the engine with a ramp under the M8 condition is summarized in Figure 6.[3] Thrusts of 932 N at $\Phi = 1$ and of 1009 N at the thermal-choking limit are attained with concentrated combustion at the throat. When the distributed combustion is postulated downstream of the throat, ΔF increases as shown by the broken line in Fig. 6. Measured thrust increases proportional to the fuel supply and reaches the maximum ΔF_{exp} of 510 N at $\Phi = 1.2$. Then it decreases in $\Phi > 1.2$ as indicated by the open diamond. The gradual diminishment of ΔF_{exp} is caused by intrusion of a high pressure region produced by combustion into the compression surface of the inlet.

Evaluation at $\Phi = 1.2$ in Fig. 6 yields ΔF_{exp} = 510 N and ΔF_{1D} = 1009 N, and the $\eta_{\Delta F}$ is 51%. This lower value compared with the case with the strut (74%) is attributed to the poor mixing of H_2 in

the ramp engine. The combustor section of the strut engine is divided into two narrow passages with 12-mm-wide and 250-mm-high, and the H_2 is injected from the 12 orifices on each side in the direction of the narrow 12-mm width. On the other hand, the ramp engine has one passage of 70-mm-wide and 90-mm-high and H_2 is injected from three orifices on each side in the direction of the 35-mm width. The penetration lengths of the sonic H_2 jets is insufficient in the 35-mm flow passage and the mixing of H_2 is retarded in the ramp engine.

As shown in the case III of Table 1 and Figure 6, however, the D_{int} of the ramped engine is small, i.e., 295 N. Consequently, the maximum ΔF_{net} is found to be 215 N at Φ = 1.2. The theoretical ΔF_{net} is evaluated to be 915 N from the minimum drag of 90 N. Comparison of two ΔF_{net} yields a η_{net} of 23%. The positive ΔF_{net} in the ramp engine is due to the small D_{int} and the extension of the operational range to Φ = 1.2. However, the net thrust performance is not sufficient. The case III in Table 1 indicates that the net Isp is about 4 km/s. The lower $\eta_{\Delta F}$ of 51% implies that the combustion efficiency must be doubled. The η_{net} of 23% suggests that the specific impulse may be raised to 17 km/s by improvement of the combustion performance and the drag performance.

Effects of Boundary Layer Ingestion

Effects of swallowing of the boundary layer by engines were examined by moving the engines into the core flow in the facility nozzle in the M8 testing.[4] Figure 7 summarizes the engine data and the theoretical performances, the solid lines denoting the ΔF by the engine with the 46-mm-thick strut and the broken lines denoting ΔF by the ramp engine. The airflow rate in the engines increases by 15% as shown in the case II of Table 1 when the engines are moved into the core region of the facility nozzle. Therefore, the thrust by the engine excluding the boundary layer increases by 15% at a given Φ. The reason why the ΔF_{1D} by the engines with the strut or the ramp in Fig. 7 are greater than that in Fig. 5 or 6 is due to this increase of their mass flow rates. Similarly, the reason that the ΔF_{1D} by the strut engine is lower than that by the ramp engine in Fig. 7 is the lower η_c in the strut engine (the case II and IV in Table 1). The subscale wind tunnel testing confirmed that the moving of engine into the core flow had negligible effects on the η_p and the D_{int} of engines.[7]

When the engine with the 46-mm-thick strut swallowed the boundary layer on the facility nozzle, it fell into inlet unstart at Φ = 0.4 as shown in Fig. 5. However, the solid circles in Fig. 7 indicate that the engine operates up to Φ = 2.1 when the boundary layer is excluded. The maximum ΔF_{exp} measured is 1220 N and the $\eta_{\Delta F}$ is found to be 92% by comparison with the ΔF_{1D} of 1330 N at Φ = 2.1. With exclusion of the boundary layer, the strut engine can produce ΔF_{net} of 560 N and the η_{net} is 45%. On the other hand, although the operational range in the ramp engine is not drastically improved, the maximum ΔF_{exp} increases from 510 N (Φ = 1.2) to 760 N (Φ = 1.3) and the ΔF_{net} is doubled to 465 N.

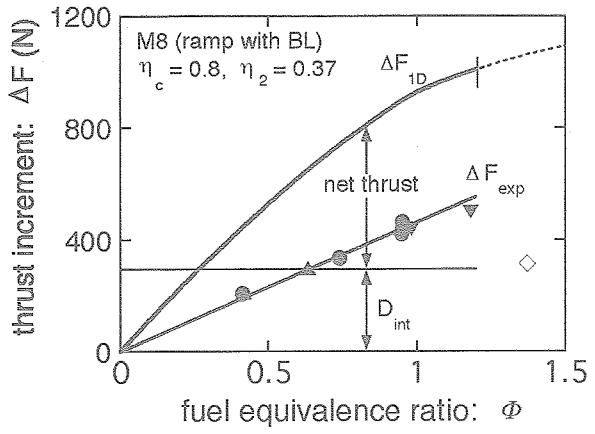

Fig. 6 Measured thrusts and the comparison with analytical value (M8 - ramped engine).

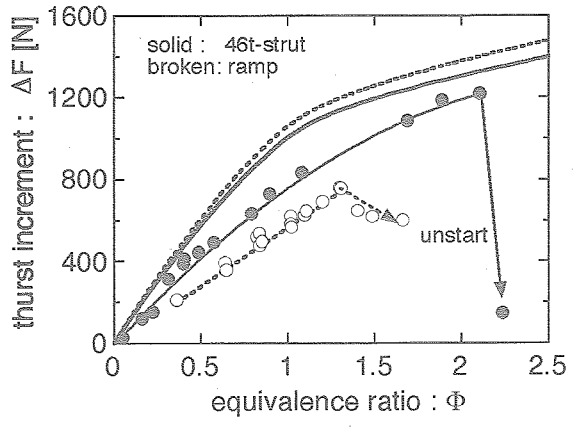

Fig. 7 Effects of boundary-layer exclusion in the struted and ramped engines (M8)

Mach 6 Condition

The test data in the M6 condition are illustrated in Fig. 8.[6] In these experiments, a 30-mm-thick strut was installed in the engine. The combustion switches from a weak mode (flame blown-off to the downstream section) to an intense mode (flame anchored in the combustor) and causes a jump in thrust near $\Phi = 0.3$. Above $\Phi = 0.3$, the engine operates in the intense combustion mode and exhibits a hysteresis between two combustion modes. When the boundary layer was not bled, the engine fell into the unstart at $\Phi = 0.48$ just after attaining the maximum thrust of 1620 N. Thus the limit fuel rate in the baseline engine was $\Phi = 0.48$ without the bleed.

Figure 8 shows that the bleed of 30 g/s (0.6% of captured air in the engine) extends the start limit from $\Phi = 0.48$ to $\Phi = 1$ to deliver the maximum thrust of 2460 N. As shown in Fig. 2, the engine switched to the unstart condition during the test at $\Phi = 1$. The limit of $\Phi = 1$ is on the boundary of start/unstart conditions. By subtracting the D_{int} of 784 N, the ΔF_{net} is 1676 N and the fuel Isp is calculated to be 11.6 km/s as shown in the case VI of Table 1.

The achievement factors of the thrust and the net thrust were evaluated by comparisons with analysis. The air capture ratio of the engine was 0.80 and the total pressure recovery factor at the combustor was 0.32.[8] The lowered η_p caused thermal choking at the engine throat at $\Phi = 0.4$. In Figure 8, the theoretical curve is estimated by assuming the distributed combustion in $\Phi > 0.4$. Since the ΔF_{1D} at $\Phi = 1$ is 4070 N as indicated in the case VI of Table 1, the $\eta_{\Delta F}$ and ηnet become 60% and 44%, respectively. These achievement factors suggest that the Isp may be raised to 19.3 km/s by improving the combustion performance and to 26 km/s by improving the drag performance of the engine in addition to the combustion.

In the M4 tests as discussed in the next section, the two-staged injection of H_2 extended the engine start limit and increased the maximum thrust. However, it did not improve the thrust performance in the M6 condition. This is attributed to limited residence time of fuel in the engines. Since the second injectors are located 462 mm upstream of the engine exit, the residence time of fuel injected the second injectors is not sufficient for the mixing and combustion. Optimum studies on the injector locations are required in the multi-staged combustors for scramjet engines.

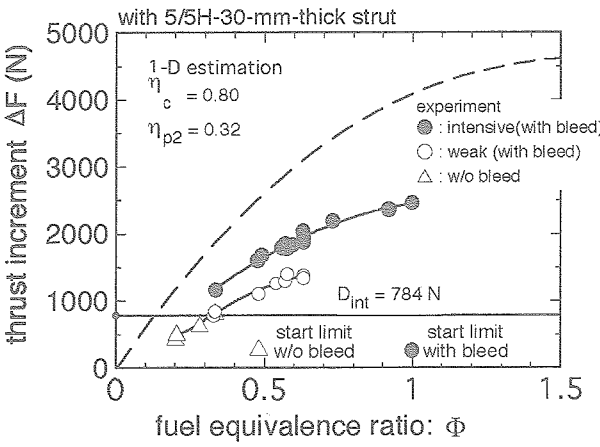

Fig. 8 Measured thrusts and the comparison with analytical value (M6 - struted E1 engine)

Mach 4 Condition

Figure 9 shows a comparison of ΔF_{1D} and ΔF_{exp} measured in the engine with neither struts nor ramp ($\varepsilon = 2.86$).[5] Because the incoming flow Mach number is as low as 3.4, the engine is easily thermally-choked at $\Phi = 0.1$ if concentrated combustion at the throat is assumed. Therefore, the distributed M1 combustion in the downstream section of the engines is assumed in $\Phi > 0.1$ in Fig. 9. The ΔF_{1D} increases from 2250 N at $\Phi = 0.3$ to 3650 N at $\Phi = 1$. With increasing Φ, the combustion region is moved down to the engine exit and the high pressure area generating thrust is confined to the narrow section near the nozzle. For instance, the engine thermally-chokes at the engine exit at $\Phi = 1$, when the combustion efficiency is higher than 70%. The saturated behavior in the ΔF_{1D} in Fig. 9 is attributed to this limited thrust surface.

The open symbols in Fig. 9 denote baseline data obtained in the engine and the solid symbols are for the engine with boundary layer bleed and two-staged injection of H_2. The switching of combustion modes is observed at $\Phi = 0.2$ at which

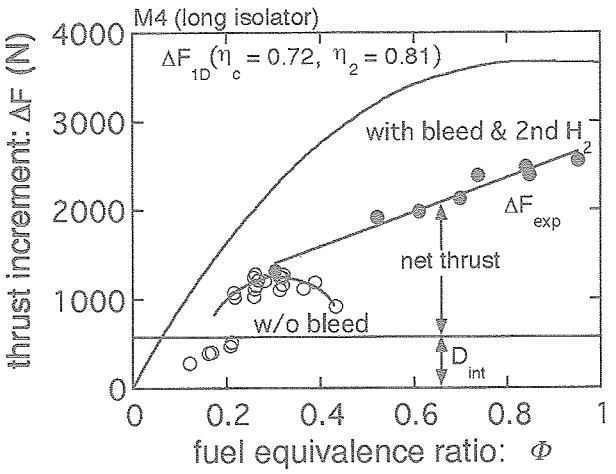

Fig. 9 Measured thrusts and the comparison with analytical value (M4 E1 engine without strut).

the ΔF_{exp} jumps from 500 N to 1000 N. The engine without bleed attains a maximum ΔF_{exp} of 1200 N at $\Phi = 0.3$ and the ΔF_{exp} gradually diminishes $\Phi > 0.3$. This diminished ΔF_{exp} is caused by the intrusion of high pressure into the inlet. Since the D_{int} of the baseline engine is 570 N (the case VII in Table 1), the ΔF_{net} is 630 N and the Isp is 10.8 km/s. The $\eta_{\Delta F}$ and η_{net} are 53% and 32%, respectively, where the Df_0 is evaluated to be 280 N.

There are two reasons for this poor η_{net} in the engine. The first is the large Dp in the internal drag. As discussed later, the Df is near the lowest limit and it is difficult to further decrease it. The spillage drag governs the Dp at the lower Mach number and must be optimized in the engine. The second reason is that the start range is restricted to less than $\Phi = 0.3$ leading to a small thrust value. To extend engine operational range, two methods were tested in the Mach 4 engine, namely the boundary layer bleed and the two-stage injection of H_2. A porous plate was installed which extended from the exit of the inlet to the isolator section on the topwall. Suctioned air of 200 g/s (3% of engine airflow) was measured by an orifice in the bleed device and exhausted to the test cell. Tomioka et al reported that two-stage injection was effective for moderating of the pressure rise in the combustor and retarding the inlet unstart.[10] In engine tests, the second injectors were located 558 mm downstream of the step in the combustor (462 mm upstream of the engine exit). The second H_2 was perpendicularly injected from orifices on the sidewalls.[5]

Effects of the bleed and the second injection are shown by the solid symbols in Fig. 9, where the engine operates up to $\Phi = 0.95$ and the maximum ΔF_{exp} increases from 1200 N to 2560 N. Although bleed of 200 g/s increased the D_{int} from 570 N to 700 N, the ΔF_{net} was improved from 630 N to 1860 N. The Isp is found to be 10 km/s. This Isp lower than the Isp (10.8 km/s at $\Phi = 0.3$) in the baseline engine is attributed to two factors: the thrust data near $\Phi = 1$ and the poor combustion efficiency of the secondarily-injected H_2. The maximum Isp resulting from the bleed without the second injection was found to be 12.4 km/s at $\Phi = 0.66$.

Table 1(case VII and VIII) shows that the $\eta_{\Delta F}$ is improved from 53% to 70% and that the η_{net} becomes from 32% to 55% as the result of bleeding and the two-staged injection of H_2. The combustion efficiency in the lower Φ region is high, because the $\eta_{\Delta F}$ is 80% at $\Phi = 0.25$. It is easy to improve the combustion efficiency of the secondarily-injected H_2 in larger flight-type engines. The mixing and combustion in external nozzles in vehicle aftbodies also promise to result in better combustion because the residence time becomes greater there.

In the last part of this section, the accuracy of the two assumptions, namely the complete mixing of H_2 by the entrance of the combustor and the distributed combustion, are examined based on our wall pressure distribution data (Fig. 10). In Fig. 10, the wall pressure nondimensionalized by q_1 is plotted with the distance from the engine leading edge. The stepwise increase of sidewall pressure is calculated by a swept shock inlet analysis. A one-dimensional flow analysis for airflow ($\Phi = 0$) and three analyses for combustion cases ($\Phi = 0.3$, 0.5 and 0.8) are illustrated by solid lines.

Measured wall pressure during combustion is indicated by open triangles (for the topwall) and circles (for the side wall). Open circles denote the pressure distribution before the injection of H_2.

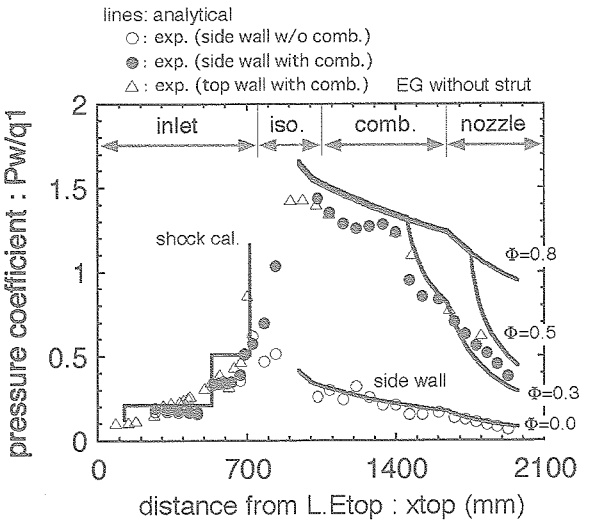

Fig. 10 Comparison with wall pressure assuming M1 combustion in the combustor (M4).

Solid circles show the pressure with combustion. Wall pressure without combustion rises to 1 at the inlet exit and decreases from 0.4 at the isolator to 0.08 at the engine exit. One-dimensional analysis well simulates this pressure distribution. With fuel equivalence ratio of 0.3, the engine distributes combustion from x = 800 to 1400, where the H_2 burns with maintenance of M1 in the diverging combustor section. The combustion of H_2 of Φ = 0.3 is completed at x = 1400 and the combustion gas isentropically expands to the engine exit. The wall pressure decreases from 1.3 to 0.2. With increasing Φ, the distributed combustion region is extended and the M1-combustion region occupies the region up to the engine exit for Φ = 0.8.

The engine data for a two-staged injection of Φ = 0.95 (Φ = 0.54 from the first injectors and Φ = 0.41 from the second injectors) show that the pressure rises from 0.5 to 1.5 at the throat. The experimental pressure distribution varies along the theoretical curves for combustion of Φ = 0.3 to the combustor. This implies that H_2 injected from the first injectors is well mixed and that the bulk combustion efficiency is fairly high. The wall pressure downstream of the combustor decreases to 0.4 along the theoretical curve for $0.3 < \Phi < 0.5$. Comparison of these experimental data and the theoretical curves suggests that the bulk combustion efficiency is about 50%, which agrees with the $\eta_{\Delta F}$ of 53% in the case VII of Table 1. Thus the fast mixing of H_2 injected into the combustor and the distributed combustion are confirmed to be good and realistic assumptions for combustion in our scramjet engines.

Drag Performance of Engines

The net thrust is governed by the magnitude of the D_{int}. Figure 11 presents the dependencies of D_{int} on the flight Mach numbers and the engine geometries.[9] The drag is expressed as drag coefficients defined by using the q_1 and the engine inlet area (A_1). For instance, the column on the far-left shows the breakdown of the C_{int} in the strutless engine (ε = 2.86) in the M4 condition. The Cdp and Cdf are 0.061 and 0.054, and their sum yields C_{int} of 0.115. It was impossible to stabilize combustion in an engine without struts in the M6 flight condition. The flameholding was achieved by a 30-mm-thick, 1/5H-high strut. The 30-mm-thick, 5/5H-high strut further improved the combustion performance as shown in the previous section. However, in Fig. 11, the Cdf is doubled and the C_{int} is increased to 0.150 by the strut.

The higher Mach number decreases the Cdp in the engine. For instance, when the 30-mm-thick strut is installed in the M8 condition, the C_{int} becomes 0.133, 80% of it being Cdf. Since the strut was found to be insufficient for the M8 combustion,

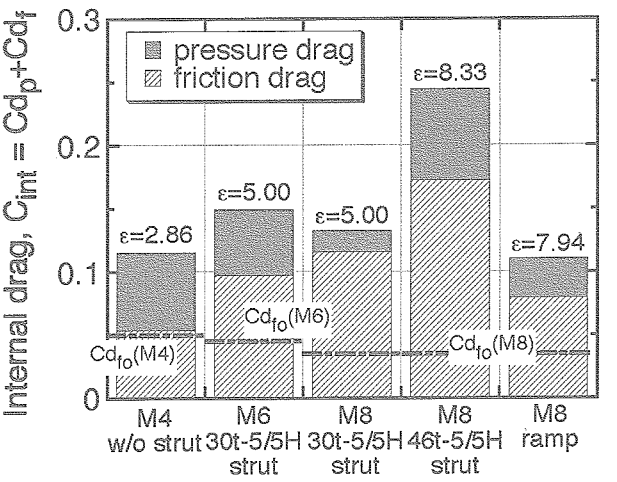

Fig. 11 Breakdowns of friction and pressure drags in the internal drag.

the 46-mm-thick strut was employed to attain the better combustion performance. This large strut with $\varepsilon = 8.33$, however, increases the Cdp and Cdf and consequently doubles the C_{int} coefficient to 0.244. This is the reason why the engine cannot deliver the net thrust as explained in Fig. 5. The column on the far-right shows the C_{int} breakdown drag of the ramp engine in the M8 condition. Although the engine has an $\varepsilon = 7.94$, nearly equal to that in the engine with the 46-mm strut, the C_{int} decreases to less than half and is smaller than that with the 30-mm-thick strut ($\varepsilon = 5$). This is attributed to the reductions in the base drag and the wet surface area of the strut.

Achievement Factor for Drag Performance

An estimation of the minimum drag is necessary to discuss the magnitudes of the D_{int} and to quantify the achievement of drag reduction. An ideal engine, which is comprised of an isentropic compression inlet and an isentropic expansion downstream of the throat, is assumed. No pressure drag is produced in the engine. However, there is the friction drag. The minimum friction drag (Df_0) can be estimated from an engine duct consisting of four flat plates with geometry similar to that of the engine. The Df_0 of the internal walls is calculated for a duct with a width (W), a height (H) and a length (L). The η_{drag} is defined as a ratio of the Df_0 and the D_{int} measured in the test engines.

$$\eta_{drag} = Df_0 / D_{int} \tag{3}$$

$$Df_0 \equiv c_f \cdot A_{wet} \cdot q_1 \tag{4}$$

$$c_f = 0.472\left(\log Re_L\right)^{-2.58} \Big/ \left(1+\frac{\gamma-1}{2}M_1^2\right)^{0.467} \tag{5}$$

$$A_{wet} = 2(H+W)\cdot L \tag{6}$$

The η_{drag} is an indicator of how close the test engines are to the ideal engine with no wave drag.

The η_{drag} is evaluated from the minimum friction drag in Table 1 and Fig. 11. The Cdf_0 are indicated by the horizontal, broken lines in Fig. 11. In the M8 condition, the η_{drag} in the engine with the 30-mm-thick strut is 0.29. The replacement with the 46-mm-thick strut lowers it to 0.14. This poor η_{drag} causes the negative net thrust in Fig. 5. The large strut has a Cdf of 0.172, which is five times greater than the Cdf_0 of 0.038 in the rectangular duct. This large Cdf is caused by the large wet area and the increases of dynamic pressure and the wall friction coefficient. Replacing the strut with the ramp improves a η_{drag} from 0.14 to 0.31. The Cdf is halved from 0.172 to 0.079 and the Cdp decreases from 0.072 to 0.041.

In the M4 condition, the strutless engine indicates a small Cdf of 0.057, which is comparable to the Cdf_0 in the rectangular duct (0.052). This means that the engine is close to the rectangular duct and it is impossible to decrease the Cdf any further. On the other hand, the Cdp is found to be 0.061. The large spillage of air in the inlet in the M4 condition is responsible for the large Cdp. As the result, the η_{drag} is found to be 0.49. The C_{int} may be halved by minimizing the Cdp. The spill rate and the additive drag produced by the spilled flow have to be optimized in inlet designs to improve the η_{drag} and the η_{net} in lower Mach number flights.

Summary

Baseline thrust performance was estimated by one-dimensional analysis to quantify the thrust, the net thrust and the drag performances attained in our engine tests from Mach 4 to Mach 8. Comparisons with the engine test data lead the following conclusions.

1) The engine with a ramp compression inlet delivered a maximum thrust of 510 N and a net thrust of 215 N in the M8 condition. Comparison with the theoretical thrust and the minimum drag yields thrust and net thrust achievement factors of 51% and 23%, respectively.
2) Exclusion of the boundary layer extended the engine operational range from $\Phi = 0.4$ to $\Phi = 2.1$ and produced a maximum thrust of 1220 N and a net thrust of 560 N. This improved the thrust and net thrust factor to 92% and 45%, respectively.

3) The baseline engine with a 30-mm-thick, 5/5 H-high strut showed a thrust of 1620 N under the M6 condition. The thrust and net thrust factors were 64% and 37% in the engine without the boundary layer controls.
4) The engine without struts in the M4 condition operated with distributed combustion in $\Phi >$ 0.1. The thrust factor was 53% and the net thrust factor was as low as 32% due to the large pressure drag. The pressure drag should be minimized by optimizing the spillage of the inlet in lower Mach number flights.
5) The boundary layer bleed of 3% air and the two-stage combustion in the M4 condition increased the thrust 3-fold and attained a maximum net thrust of 1860 N (Isp = 10 km/s). The thrust and the net thrust achievement factors were evaluated to be 70% and 55%. Under the M6 condition, the 0.6% bleed increased the thrust from 1620 N to 2460 N and doubled the net thrust.

Reference

1. Chinzei, N., Mitani, T. and Yatsuyanagi, Y., "Scramjet Engine Research at the National Aerospace Laboratory in Japan," Scramjet Propulsion, edited by Curran, E. T. and Murthy, S. N. B., Vol. 189, Progress in Astronautics and Aeronautics, AIAA, New York, 2001, pp159-222.
2. Kobayashi, K., Tomioka, S., Kanda, T., Tani, T., Hiraiwa, T., and Saito, T., Modified Water-cooled Scramjet Engine Tested under M8 Condition, AIAA Paper 2001-3202, 2001.
3. Hiraiwa, T., Kanda, T., Mitani, T. and Enomoto, Y., "Experiments on a Scramjet Engine with Ramp-Compression Inlet at Mach 8 condition," AIAA Paper 2002-4129, presented at the 38th Joint Prop. Conf., Indianapolis, 2002.
4. Hiraiwa, T., Kanda, T., Kodera, M., Saito, T., Kobayashi, K., Kato, T., Effect of Induced Boundary Layer on Scramjet Engines' Thrust and Combustion Characteristics, AIAA 2003-4739, presented at 39th Joint Prop. Conf., 2003.
5. K. Kobayashi, S. Tomioka, T. Hiraiwa, K. Kato, T. Kanda, and T. Mitani, "Suppression of Combustor-Inlet Interaction in a Scramjet Engine under M4 Flight Condition," AIAA 2003-4737, presented at 39th Joint Prop. Conf., 2003.
6. Kodera, M., Tomioka, S., Kanda, T. and Mitani, T., Mach 6 Test of a Scramjet Engine with Boundary-Layer Bleeding and Two-Staged Fuel Injection, to be presented at the 12th Spaceplane Conference, Norfolk, 2003.
7. Kouchi, T., Mitani, T., Hiraiwa, T., Tomioka, S., Masuya, G., Evaluation of Thrust Performance in Kinetic-Controlled Scramjet Engines with Measured Internal Drag, submitted to Journal of the Japan Society for Aeronautical and Space Science, 2003 (in Japanese).
8. Mitani, T., Hiraiwa, T., Tarukawa, Y., and Masuya, G., Drag and Total Pressure Distributions in Scramjet Engines at Mach 8 Flight, Journal of Propulsion and Power, Vol.18, No.4, 2002, pp.953-960.
9. Mitani, T., Izumikawa, M., Watanabe, S., Tarukawa, Y., Force Measurements of Fixied Geometry Scramjet Engines from Mach 4 to 8 Flight Condition, AIAA2002-5351, 2002.
10. Tomioka, S., Murakami, A., Kudo, K. and Mitani, T., Combustion Tests of a Staged Supersonic Combustor with a Strut, J. Prop. and Power, vol. 17, No. 2. pp293-300, 2001.

JAXA Research and Development Report
(JAXA-RR-03-020E)

Date of Issue : March 25, 2004

Edited and Published by :
Japan Aerospace Exploration Agency
7-44-1 Jindaiji-higashimachi, Chofu-shi,
Tokyo 182-8522 Japan

Printed by :
BCC Co., Ltd.
2-4-1 Hamamatsu-cho, Minato-ku, Tokyo 105-6114 Japan

Japan Aerospace Exploration Agency